Materials Science in Semiconductor Processing 83 (2018) 70–82

Contents lists available at ScienceDirect

Materials Science in Semiconductor Processing

journal homepage: www.elsevier.com/locate/mssp

Neodymium doped TiO_2 nanoparticles by sol-gel method for antibacterial and photocatalytic activity

N. Nithya[a], G. Bhoopathi[a,*], G. Magesh[a], C. Daniel Nesa Kumar[b]

[a] Department of Physics, PSG College of Arts and Science, Coimbatore 641014, India
[b] Hindusthan College of Arts and Science, Coimbatore 641028, India

ARTICLE INFO

Keywords:
TiO_2
Nd doped TiO_2 nanoparticles
Anatase
Rutile
Brookite phase
Antibacterial
Photocatalytic activity

ABSTRACT

In the present study, TiO_2 and Nd doped TiO_2 nanoparticle was synthesized through Sol-gel method with different molar ratio and different starting material. The synthesized nanoparticle was characterized by XRD, UV-Vis, PL, FE-SEM, HR-TEM, and EDS analysis. The X-ray diffraction pattern confirms tetragonal anatase phase with average crystallite size of 14–10 nm. The influence of phase transition was identified by the addition of dopant Nd. The calculated band gap is in the range of 3.48–3.44 eV. Near UV and blue emission in PL spectrum indicate the presence of crystal defects in TiO_2 lattice. The structural morphology of the prepared sample was analyzed by FESEM. The average particle size of the sample was determined by TEM analysis. The elemental compositions and incorporation of Nd ions into the TiO_2 nanoparticles was detected by using energy dispersive spectra analysis. The antibacterial activity of pure TiO_2 and Nd doped TiO_2 nanoparticle was tested for different bacterial organisms like Escherichia coli (Gram-negative) and staphylococcus aureas (Gram-positive) bacteria. The photo catalytic activity of the prepared samples on degradation of Methylene Blue and Congo Red under ultraviolet irradiation were also studied.

1. Introduction

The environmental issues and industrialization increasingly attracted more attention for developing new ecofriendly water purification technologies. The release of dye-polluted wastewater by textile industries causes environmental problems. Synthetic organic dyes are mainly used in the textile industry; the removal of organic and inorganic dyes is a challenging one. The application of nanotechnology results in wastewater treatment owing to large surface area to volume ratio of nanomaterials [1]. The semiconductor photocatalysis has emanated as promising technology used for wastewater treatment, degradation of organic and inorganic pollutants in water. The application of photocatalysis is in the field of microbiology and agriculture because it is biologically inert and non- toxic. The antimicrobial agents are promising materials such as Nano sized metals and metal oxides. The metal oxide received more recognizing over past decade due to less toxicity, greater selectivity etc. antimicrobial agents are used in many industrial sectors including environmental, wastewater treatment, food packaging, textile and medical care [2]. In the metal oxide semiconductors, ZnO, TiO_2, Al_2O_3, CuO, SiO_2, Fe_2O_3 and CeO_2 are mostly used as a antimicrobial agents. Among these metal oxide semiconductors, TiO_2 is extensively used as an antimicrobial agents due to their photocatalytic activity under UV light [3].

There has been tremendous progress in the research of future nanoelectronic applications using TiO_2 nanoparticles in recent years. TiO_2 nanoparticles are highly investigated as a photo catalytic and photo electro chemical material [4]. It is also the most preferred semi conducting photocatalytic material due to its favorable properties like non-toxic, chemical inertness, stability, photosensitive etc. [5]. A growing interest in the development of well-structured, porous, high surface area, TiO_2 nanoparticles were used in many applications including building materials, medicaments production, pollutants destructions, solar energy conversion, photo catalyst, and antimicrobial activity. This application not only depends on the properties of TiO_2 but also on the crystalline structures of TiO_2 [6]. TiO_2 is usually in the forms of anatase, rutile, and brookite crystal phase. Anatase form of TiO_2 is more stable and more efficient in photo activity when compared with rutile and brookite [7].

Nowadays many studies have been devoted for the improvement of the antibacterial and photocatalytic properties of TiO_2 nanoparticles, the investigations suggests that these properties can be enhanced by doping with transition metals, non-metals,noble metals and rare earth metals [8]. The most important effects of doping are increasing the surface area, phase transformation, and particle size reduction [9].

* Corresponding author.
E-mail address: bbijju03@gmail.com (G. Bhoopathi).

https://doi.org/10.1016/j.mssp.2018.04.011
Received 22 December 2017; Received in revised form 8 April 2018; Accepted 11 April 2018
Available online 23 April 2018
1369-8001/

Doping with rare earth metals like La, Ce, Er, Pr, Gd, Nd, and Sm with TiO_2 nanoparticles is to enhance the photocatalytic and antibacterial properties. Several rare earth metals are used as a dopant for TiO_2 nanoparticles to improve the antibacterial and photocatalytic activities [10]. Neodymium is one of the element of lanthanide has obtained focus on several investigations because of its particular optical and magnetic properties and promising applications in the field of optoelectronic and magnetic devices [11]. Further, Nd doping with TiO_2 nanoparticles reduces the band gap and improves the possibilities of the photocatalytic degradation under visible light [12].

Several methods are available for the synthesis of TiO_2 nanoparticles such as hydrothermal method, solvothermal method, sol gel method, direct oxidation method, chemical vapour deposition, electro deposition, sonochemical method, and microwave method [13,14]. Among all these methods, the sol gel method is the best method because of its unique advantages including economic feasibility, simple lab equipment, less energetic conditions, possibilities of preparing powder, purity, and homogeneity [15].

Rui Tang et al., investigated the photocatalytic activity of N doped TiO_2 decorated N doped graphene composites by sol gel -method. N-RGO/N-TiO_2 composites effectively enhanced the photocatalytic activity than pure TiO_2 [16]. Previous reports on Nd doped TiO_2 nanoparticles focused on optical, structural, morphological and photocatalytic properties [17]. In this present work, pure TiO_2 and Nd doped TiO_2 nanoparticles were prepared by the sol gel method. The influence of various mole fractions of Nd^{3+} ions in TiO_2 nanoparticles, structural, optical, antibacterial, and photocatalytic properties were investigated in detail.

2. Experimental details

2.1. Materials

Synthesis of pure TiO_2 and Nd doped TiO_2 nanoparticles were carried out using analytical grade Titanium (IV) Isopropoxide (Merck, 97%), Neodymium (III) acetate dihydrate (Nd $(OOCCH_3)\cdot 2H_2O$) (Merck, 98%), Sodium Hydroxide (Merck, 99%), acetic acid (Merck, 99%) and ethanol (Merck, 99%) without any purification.

2.2. Preparation of pure and Nd doped TiO_2 nanoparticles

Pure TiO_2 and Nd doped TiO_2 nanoparticles were synthesized by sol-gel technique. Titanium (IV) isopropoxide (TTIP) was dissolved in 50 ml of isopropyl alcohol with vigorous stirring to avoid agglomeration. 2 ml of acetic acid were added to the above solution under constant stirring to complete the hydrolysis. A small amount of sodium hydroxide solution was added into the solution until it reaches pH 9. The transparent sols were allowed to aged for 24 h and washed 2–3 times with ethanol, distilled water and sodium hydroxide solution to remove metal ions present in the sols. Then the transparent sols were centrifuged at 8000 rpm for 15 min. Finally, the precipitate was dried at 120 °C for two hrs and annealed at 600 °C for 3hrs to obtain TiO_2 nanoparticles [18]. Nd doped TiO_2 nanoparticles were synthesized by same method as followed for the preparation of TiO_2 nanoparticles, except isopropyl alcohol was used as solvent for required amount of Neodymium(III) acetate dehydrate with different molar ratio (0.5 mM, 1.0 mM, 1.5 mM, 2.0 mM) and concentration of acetic acid was changed for hydrolyis.

3. Characterization techniques

Crystalline structure of the prepared samples were investigated using a powder X- ray diffractometer (PANa-lytical X′ Pert Pro) with Cu-Kα radiation source (wavelength: 1.5418 Å) and operating voltage and current was maintained at 45 kV and 30 mA respectively. The UV-Visible absorption spectra of prepared samples were recorded using JASCO (V-770, Japan) spectrophotometer. A PL spectrum was recorded at room temperature using JASCO spectroflurometer (Model FP8300, Japan) equipped with Xenon lamp. Field Emission Scanning Electron Microscope (ZEISS EIGMA) and High Resolution Transmission Electron Microscope (JOEL JEM- 2010) examined the size and morphology of the prepared samples. Energy Dispersion Spectrometer was used to carry out the elemental analysis using JOEL JEM- 2010.

3.1. Antibacterial assay

The pathogens Staphylococcus aureus and Escherichia coli were obtained from the Microbiology Laboratory, Kovai Medical Centre and Hospital, Coimbatore, South India. Kirby – Bauer disk diffusion method were performed against human pathogenic bacteria such as staphylococcus aureas (Gram positive) and Escherichia coli (Gram negative) for an antibacterial disk susceptibility tests. The standard inoculums is inoculated in the plates were prepared by dipping a sterile in the inoculums and poured on the petri dishes. After solidification, the petri dishes were spread with bacteria 2–3 times by rotating the plates at 60° to ensure homogenous distribution of inoculums. The inoculums were left to dry at room temperature with the closed lid. After inoculation, sterile discs stacked with prepared nanoparticles (100 µg of prepared samples) and standard ciprofloxacin (10 µg) were placed in the petri dish with the help of sterile forceps. Then the petri plates were incubated at 37 °C for 24 h. After incubation, the Zone of inhibition was measured in terms of diameter.

3.2. Measurement of photo catalytic activity

The photocatalytic activity of as prepared pure TiO_2 and Nd doped TiO_2 nanoparticles were analyzed by measuring the degradation rate of Methylene Blue(MB) and Congo Red(CR) dye solution using a photo reactor with two 20 W ultraviolet (UV) lamps which was used as the UV source for irradiation. In this experiment, 20 mg of pure TiO_2 and Nd doped TiO_2 nanoparticles were added to 100 ml of dye solution (40 mg/L) placed in a glass beaker. In each experiment, the solutions were stirred for 30 min under dark conditions to assure the formation of adsorption and desorption equilibrium of dyes on the pure TiO_2 and Nd doped TiO_2 nanoparticles, then the solution was irradiated under UV light. The pH of the solution was neutral. At 15 min interval, 10 ml of the solution was extracted from the solution and color removal of dye solution was determined by using UV- Vis spectrophotometer. UV-Vis spectroscopy was used to analyse the absorption changes, which is dependent to time between 400 and 800 nm. All these experiments were done at room temperature.

4. Results and discussion

4.1. Structural analysis

Fig. 1(A) shows the XRD pattern of as prepared TiO_2 nanoparticle. The determined characteristics 2Θ values are 25.37°, 37.87°, 48.13°, 54.22°, 55.10°, 62.85°, 68.80°, 70.25° and 75.22° and corresponding hkl plane values are (1 0 1), (0 0 4), (2 0 0), (1 0 5), (2 1 1), (2 0 4), (1 1 6), (2 2 0) and (2 1 5) respectively. All the diffraction peaks were well matched with JCPDS Card no. 89-4921. All the diffraction peaks are corresponding to tetragonal anatase phase of TiO_2 nanoparticle. Fig. 1(B-E) shows the XRD pattern of Nd doped TiO_2 nanoparticles with different concentration of dopant Nd. From the XRD pattern of Nd doped TiO_2 nanoparticle, the separate peak at 31.78 (1 2 1) indicates the presence of Brookite phase of TiO_2 and it is excellent agreement with the JCPDS Card no. 21-1272. The peaks at 45.48 (2 1 0) and 55.10 (1 1 0) correspond to rutile phase of TiO_2 nanoparticles. In TiO_2 and Nd doped TiO_2 nanoparticles, anatase phase is the prominent crystallite phase. The XRD pattern of TiO_2 nanoparticles has anatase crystalline phase. When Nd doped with TiO_2 nanoparticles, new peaks and shifts in

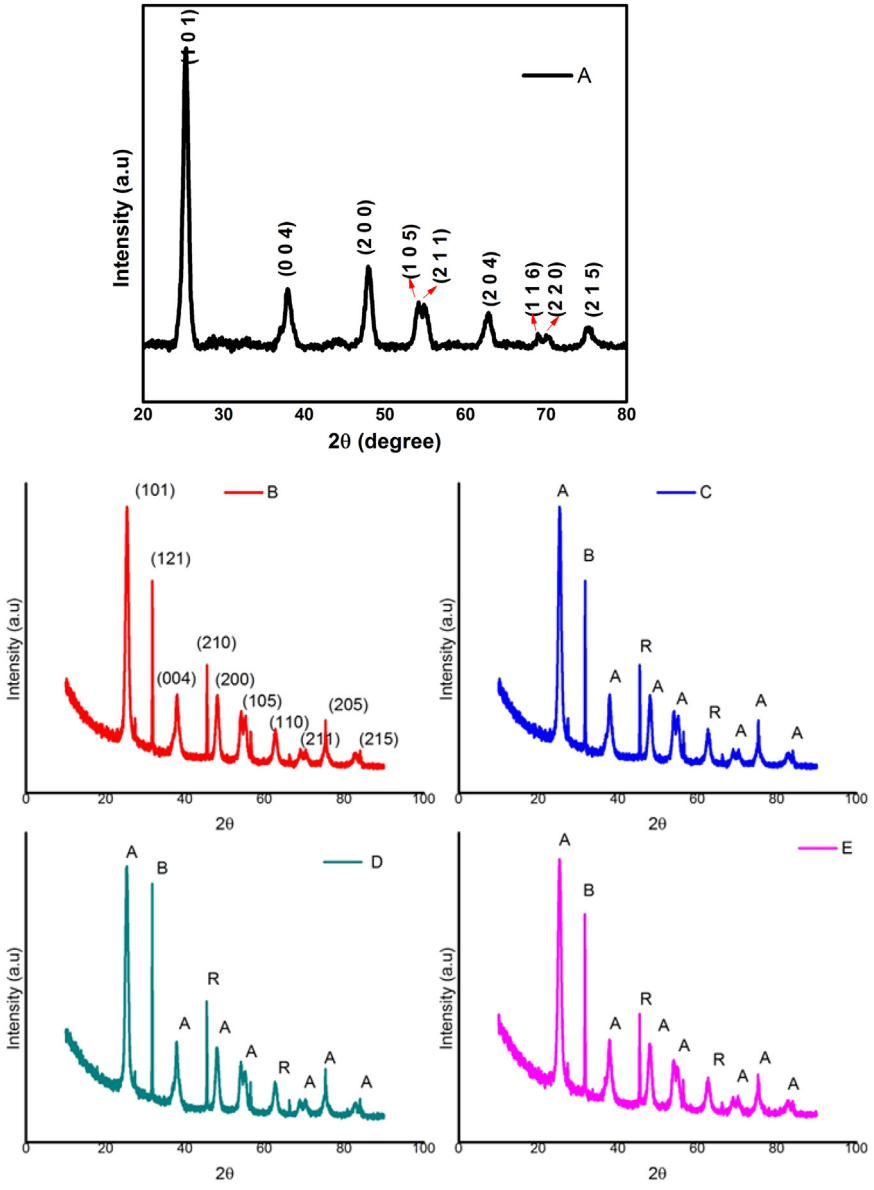

Fig. 1. (A) XRD pattern of Pure TiO_2 Nanoparticle. XRD pattern of (B) 0.5 mM of Nd (C) 1 mM of Nd (D) 1.5 mM of Nd (E) 2 mM of Nd doped TiO_2 Nanoparticles.

prominent peaks were observed. This may be assigned to the fact that the neodymium ions were dispersed well on the surface of TiO_2 nanoparticles. The shifts in peaks were also caused by defects in the crystal lattice and differ in ionic radii of metals [19].

The mass percentage of Anatase (W_A), Rutile (W_R) and Brookite (W_B) were calculated from the following equation.

$$W_A = \frac{K_A A_A}{K_A A_A + A_R + K_B A_B} \quad (1)$$

$$W_R = \frac{A_R}{K_A A_A + A_R + K_B A_B} \quad (2)$$

$$W_B = \frac{K_B A_B}{K_A A_A + A_R + K_B A_B} \quad (3)$$

where K_A and K_B were coefficient with values 0.886 and 2.721. A_A, A_R and A_B indicates the highest intensities of Anatase, Rutile, and Brookite phases [20].

The pure TiO_2 nanoparticle contains 100% anatase phase, there is no rutile and brookite phase. It might be due to the presence of minimum amount of oxygen vacancies in TiO_2 nanoparticles during particle growth, inhibit the transformation of anatase to rutile and brookite phase [21]. While in XRD pattern of Nd doped TiO_2 nanoparticle shows the mixture of anatase, rutile and brookite phase of TiO_2 nanoparticle. The mass fraction of Anatase phase was decreased when doping concentration of Nd increases. When Nd doped with TiO_2 nanoparticles, the phase transformation of nanoparticle occurs, this might be due to change of acid concentration and temperature [22]. Acid concentration and temperature has major factors affecting the phase transformation because the kinetics of reaction takes place was changed and the amount of OH- was varied by acid concentration and temperature [23].

The average crystallite size of prepared nanoparticles were calculated using Debye- Scherer's equation for anatase diffraction peaks [24],

$$D = \frac{K\lambda}{\beta \cos\Theta} \quad (4)$$

where D is the crystallite size, λ is the wavelength of X- ray radiation (0.1541 nm), K is the constant usually taken as 0.89, and β is the peak width at full wave maximum. The calculated crystallite size and physical parameters of prepared samples are shown in the Table 1. The

Table 1
Structural parameters of Pure TiO_2 and Nd doped TiO_2 Nanoparticles.

S.no	Nd concentration	2Θ	Crystallite size (nm)	Anatase	Rutile	Brookite	Lattice Parameter		Atomic packing factor c/a
				(%)	(%)	(%)	a (Å)	c (Å)	
1	0.0 mM	25.16	14.3	100	–	–	3.721	9.532	2.561
2	0.5 mM	25.25	13.82	68	12	20	3.735	9.541	2.554
3	1.0 mM	25.35	13.12	66	11	23	3.756	9.613	2.559
4	1.5 mM	25.31	12.11	63	12	25	3.772	9.654	2.559
5	2.0 mM	25.3	9.8	60	13	27	3.797	9.687	2.551

Standard JCPDS Card no. (89-4921) a = 3.777 (Å) c = 9.501 (Å).

crystallite size of TiO_2 nanoparticle decreases, when the doping concentration of Nd increases. This is because of the adsorptions of neodymium ion inhibit the growth of TiO_2 nanoparticle. The lattice parameters of semiconducting materials are usually depends on the defects, impurity atoms, and dissimilar in ionic radii of metals [25]. The lattice parameters varies with respect to distinct ionic radii of Nd^{3+} ion and Ti^{4+} ion.

The lattice constants of TiO_2 and Nd doped TiO_2 nanoparticles were calculated using the following equation [26].

$$\frac{1}{d^2} = \frac{h^2 + k^2}{a^2} + \frac{l^2}{c^2} \tag{5}$$

where d is the interplanar distance and h, k and l are the miller indices. Moreover a and c are lattice parameters of tetragonal structure. When concentration of dopant Nd increases, the lattice parameter increases, and crystallite size decreases. In this case, c/a ratio value decreases with increasing the concentration of dopant Nd. This shows that the Nd^{3+} ion was successfully incorporated into the TiO_2 crystal lattice.

The volume (V) of the unit cell for tetragonal structure of TiO_2 nanoparticle was calculated from the following equation [27].

$$V = a^2 c Å^3 \tag{6}$$

where a and c are the lattice parameter and were estimated from the peaks with highest intensities of the patterns, that is reflection of planes (1 0 1) for anatase phase. The estimated unit cell volume for TiO_2 and Nd doped TiO_2 nanoparticles were 131.97 $Å^3$, 133.09 $Å^3$, 135.61 $Å^3$, 137.35 $Å^3$ and 139.65 $Å^3$ respectively. This shows that the unit cell volume of TiO_2 nanoparticles also increases with increasing the dopant concentration of Nd.

Further dislocation densities (δ), microstrain (ε), bond length (L) and positional parameter (u) of tetragonal TiO_2 and Nd doped TiO_2 nanoparticles were calculated by using the following relation [28].

$$\delta = \frac{1}{D^2} \tag{7}$$

$$\varepsilon = \frac{\beta COS\Theta}{4} \tag{8}$$

$$L = \sqrt{\frac{a^2}{3} + (\frac{1}{2} - u)^2 c^2} \tag{9}$$

$$u = \frac{a^2}{3c^2} + 0.25 \tag{10}$$

where a and c are the lattice parameters and u is the positional parameter.

The calculated unit cell volumes, dislocation density, strain and bond lengths were listed in the Table 2. The bond length values are found to be increasing with increase in doping concentration of Nd. This may be due to the effect of replacement of Ti^{4+} ion by Nd^{3+} ion in to the TiO_2 lattice. The average crystallite size of TiO_2 and Nd doped TiO_2 nanoparticles were found to be 14–10 nm. The common qualities of photoactive TiO_2 nanoparticles include high crystallites, small crystallite size [29]. Therefore, the smaller crystallite size of prepared nanoparticles provides good antibacterial and photocatalytic activity.

4.2. Optical absorption studies

The optical properties of pure TiO_2 and Nd doped TiO_2 nanoparticles were successfully investigated by UV-Vis absorption spectroscopy. The optical properties of as prepared nanoparticle becomes increasing more and more prominent when particle size reduced in nanoscale. The UV-Vis absorption spectra for pure TiO_2 and Nd doped TiO_2 nanoparticles with different concentration of dopant Nd is shown in Fig. 2 in the range from 200 to 800 nm wavelengths.

The absorbance value is depends on the particle size and defects in the crystal lattice. The absorption value of Pure TiO_2 and Nd doped TiO_2 nanoparticles were 356 nm, 357 nm, 358 nm, 359 nm, and 360 nm respectively. All the absorption peaks are in the visible region (> 400 nm) due to the exciton recombination at room temperature [30]. As the doping concentration of Nd with TiO_2 increases, the absorption peaks shifts to higher wavelengths (red shifted) and it further decreases the bandgap (Eg), it may be due to strain and defects in crystal lattice of TiO_2 nanoparticle. These peaks may occur due to the transition of electrons from conduction band to valence band [31]. All these factors, leads to the reduction of crystallite size of TiO_2 nanoparticle when Nd doped with TiO_2 nanoparticles, which was further confirmed by XRD results.

The bandgap energy (Eg) of Pure TiO_2 and Nd doped TiO_2 nanoparticles were calculated by using the following equation [32].

$$E_g = \frac{hc}{\lambda}(eV) \tag{11}$$

where h is the Planck's constant, c is the velocity of light and λ is the wavelength (absorption edge). The band gap energy of Pure TiO_2 and Nd doped TiO_2 nanoparticles were 3.48 eV, 3.47 eV, 3.46 eV, 3.45 eV, and 3.44 eV respectively. The calculated band gap energy was compared with standard energy of band gap of bulk TiO_2 material (3.2 eV). The band gap energy was related to the crystal structure, phase composition, particle size, and morphology of the nanoparticles [33]. The calculated band gap energy was given in the Table 3. The decrease in bandgap energy with increasing the doping concentration of Nd shows that the Nd^{3+} ion incorporated into the TiO_2 crystal lattice.

The direct band gap energy (Eg) was calculated using the following tauc plot equation [34].

$$(\alpha h\nu)^2 = B\ (h\nu - Eg)^{1/2} \tag{12}$$

where hν is the photon energy, α is the absorption coefficient and B is the constant

The $(\alpha h\nu)^2$ versus hν is shown in the Fig. 3(A-E). The estimated direct optical bandgap energy values of Pure TiO_2 and Nd doped TiO_2 nanoparticles were 3.3 eV, 3.29 eV, 3.28 eV, 3.27 eV, and 3.26 eV respectively. It found that the direct optical bandgap of TiO_2 nanoparticle decreases with increasing the concentration of dopant Nd. This attributed to the size quantization of semiconducting nanomaterial. The size

Table 2
Physical parameters of Pure TiO_2 and Nd doped TiO_2 Nanoparticles.

S.no	Nd concentration	Volume (V)(Å ^{3})	Dislocation density (δ) (line × m^{-2})	Strain (ε)	Positional parameter (u)	Bond length (L) (Å^3)
1	0.0 mM	131.97	4.890 E+14	0.0024	0.3007	2.87
2	0.5 mM	133.97	5.235 E+14	0.0025	0.3008	2.873
3	1.0 mM	135.61	5.890 E+14	0.0026	0.301	2.891
4	1.5 mM	137.35	6.818 E+14	0.0028	0.3011	2.903
5	2.0 mM	139.65	10.412 E+14	0.0035	0.3012	2.917

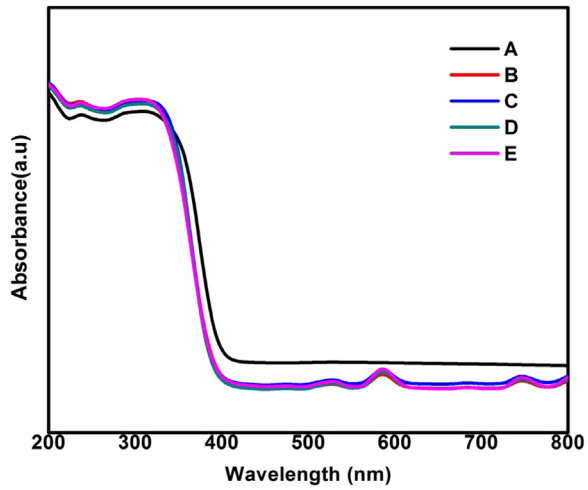

Fig. 2. UV-Vis absorption spectra of (A) Pure TiO_2 (B) 0.5 mM of Nd (C) 1 mM of Nd (D) 1.5 mM of Nd (E) 2 mM of Nd doped TiO_2 Nanoparticles.

Table 3
Calculated band gap energy values of Pure TiO_2 and Nd doped TiO_2 Nanoparticles.

S.no	Nd concentration	Wavelength (nm)	Optical bandgap energy (eV)	Bandgap energy calculated from tauc plot (eV)
1	0.0 mM	356	3.48	3.3
2	0.5 mM	357	3.47	3.29
3	1.0 mM	358	3.46	3.28
4	1.5 mM	359	3.45	3.27
5	2.0 mM	360	3.44	3.26

quantization occurs due to electron and holes confined in a certain volume of semiconducting nanomaterial. [35]. This may be assigned to the f-f or 4f transition of electrons of Nd^{3+} ion that are substituted in to the Ti^{4+} ion [36]. As a result, decrease in bandgap energy increases the photocatalytic activity of pure TiO_2 and Nd doped TiO_2 nanoparticles.

4.3. Photoluminescence studies

The optical and photo electronic properties of prepared nanoparticles were investigated by using photoluminescence spectrum. The cause of main photoluminescence emission in any semiconductor is prominently due to radioactive recombination of electrons and holes in the semiconducting metals [37]. The Fig. 4 shows the photoluminescence spectra of pure TiO_2 and Nd doped TiO_2 nanoparticles with different doping concentration of dopant Nd in the range 350–550 nm.

The PL spectra of Pure TiO_2 nanoparticles exhibit two emission peaks at 390 nm and 459 nm. The peak at 390 nm corresponds to UV emission region. This UV emission region may be due to the near band edge emission, which causes the recombination of electron and hole on the surface of TiO_2 nanoparticles. There were a lot of oxygen vacancies and defects on the surface of TiO_2 nanoparticles. Those surfaces of TiO_2 nanoparticles can easily binds to the photo induced electrons to form excitons [38]. The peak at 459 nm corresponds to blue emission, which are emerge from the overlapping of the electron in the donor level of conduction band with the holes in the valance band [39]. The PL spectra of Nd doped TiO_2 nanoparticles shows peaks at 386 nm, 387 nm, 388 nm, and 389 nm respectively. The dopant Nd does not give rise to new PL spectrum. Doping Nd ion with TiO_2 nanoparticle leads to decrease of intensity. Decrease in intensity also enhanced the charge transfer of electrons. On comparing the PL spectra of Nd doped TiO_2 nanoparticles with the PL spectra of TiO_2 nanoparticle, the peak position of UV emission region slightly shifts to wavelength region from 386 nm to 389 nm. The decrease in intensity might be attributed to the decrease in particle size of Nd doped TiO_2 nanoparticles with respect to TiO_2 nanoparticles. The result confirms that the PL intensity depends on the various concentrations of dopant Nd ions. The increase in wavelength and decrease in crystallite size usually increases the content of oxygen vacancies and exhibit good photocatalytic activity.

4.4. Morphology and compositional analysis

4.4.1. Field emission scanning electron microscope

The size and morphology of the nanoparticles were determined by using FESEM analysis. Fig. 5 shows the FESEM images of pure TiO_2 and Nd doped TiO_2 nanoparticles with heterogeneous morphology with non- uniform distribution and also irregular arrangement. The particle sizes of TiO_2 nanoparticles are agglomerated. When Nd doped with TiO_2 nanoparticles, agglomeration was reduced and it inhibited the particle size. The FESEM images reveal simple aggregation of spherical like particles with decreasing particle sizes.

4.4.2. High resolution transmission electron microscope

High Resolution transmission electron microscopy (HRTEM) was useful to understand and study the doping of neodymium ion into the TiO_2 nanoparticles. HRTEM analysis was performed to study the incorporation or distribution of dopant Nd ions into the TiO_2 nanoparticles, crystalline nature, particle size, and morphology of as prepared samples. TEM images of pure TiO_2 and Nd doped TiO_2 nanoparticles with 0.5 mM and 2 mM concentrations were shown in Fig. 6(a-c). A TEM image in Fig. 6(a-c) shows that the non-uniform distributed particles with agglomeration. The agglomeration of nanoparticles might be attributed to the combined larger and smaller particles. Because, the smaller particle size of titanium nanoparticles agglomerated with the larger particle size [40]. The particle size of pure TiO_2 and Nd doped TiO_2 nanoparticles with dopant concentration of 0.5 mM and 2 mM were found to be in nanoscale with the grain size less than 10 nm. Fig. 6(d-f) depicts the high resolution TEM images of pure TiO_2 and Nd doped TiO_2 nanoparticles with dopant concentrations of 0.5 mM and 2 mM for the analysis of lattice fringes. The results indicates that the all the prepared samples shows the uniform distribution of nanoparticles with fine crystalline nature. All the prepared nanoparticles resembles high crystalline in nature. The lattice spacing were found to be 0.4337 nm, 0.4415 nm and 0.4550 nm which represents the (1 0 1) anatase phase of nanoparticles and it was further confirmed by XRD results, while Nd with doped TiO_2 nanoparticles phase transformation occurs. However, in all the prepared samples anatase phase is the prominent peak. From the results, d-spacing value was increasing

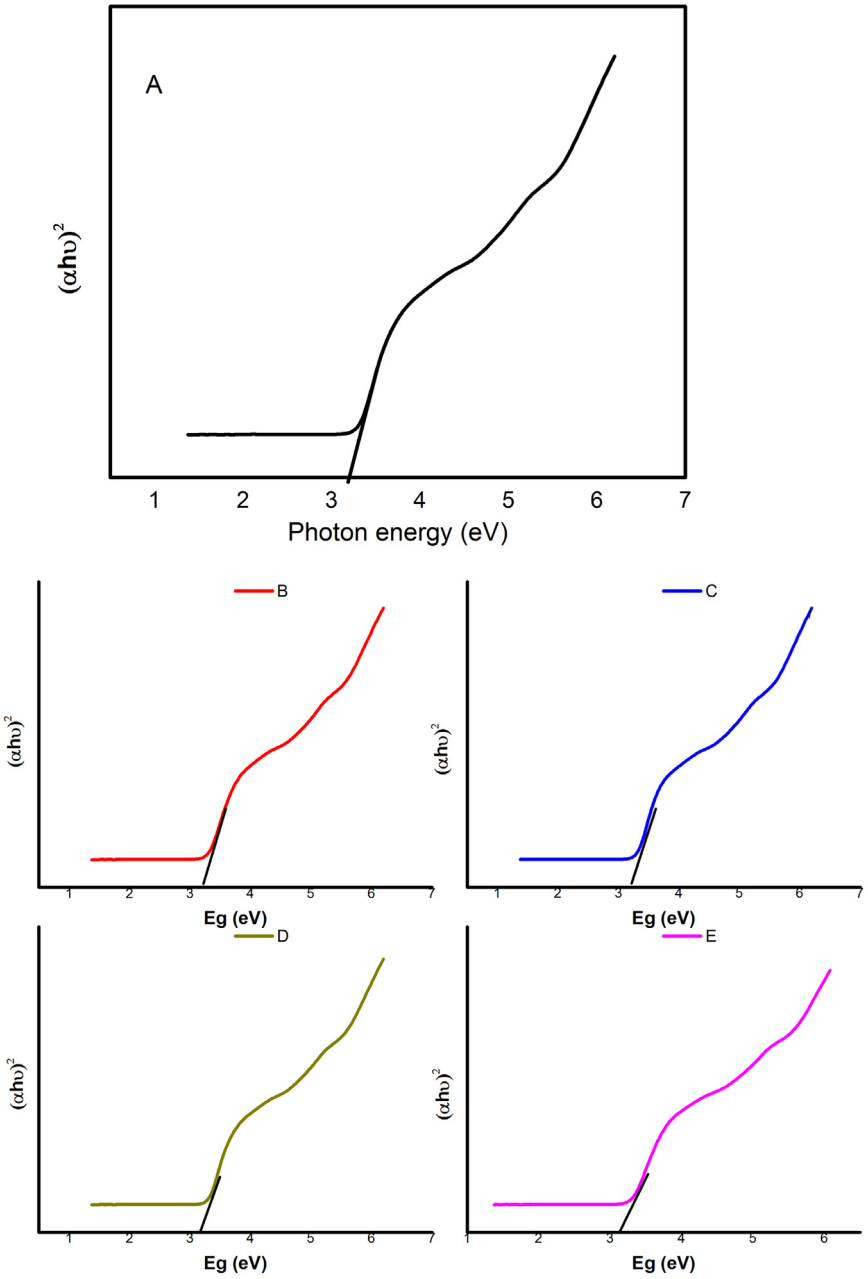

Fig. 3. (A) Tauc plot of pure TiO_2 Nanoparticle. Tauc plots of (B) 0.5 mM of Nd (C) 1 mM of Nd (D) 1.5 mM of Nd (E) 2 mM of Nd doped TiO_2 Nanoparticles.

when Nd doped with TiO_2 nanoparticles. Similar results were observed and reported in Cr doped TiO_2 nanoparticles which can be attributed to the defects when metals are doped with metal oxide nanoparticles [41].

Further, the crystallinity of pure TiO_2 and Nd doped TiO_2 nanoparticles with doping concentrations of 0.5 mM and 2 mM were examined by selected area diffraction (SAED) pattern and shown in Fig. 6(g-h) respectively. The ring pattern indicates that the all the samples were well crystalline in nature with (1 0 1) anatase phase with high intensity. All the plane values were good agreement with the XRD results. The average particle size of pure TiO_2 and Nd doped TiO_2 nanoparticles were found to be 16.34 nm, 15.12 nm and 11.82 nm respectively. The estimated particle sizes were in good agreement with the calculated crystallite size from the XRD patterns. The decrease in crystallite size, intensity of the peaks and phase transformation were observed in Nd doped TiO_2 nanoparticles.

4.4.3. EDS analysis

The contents and chemical composition of nanoparticles were studied by EDS spectra. Fig. 7(a-c) shows the EDS spectra of pure TiO_2 and Nd doped TiO_2 (0.5 mM and 2 mM of Nd) nanoparticles. The presence of Ti, Nd and O element in the sample were confirmed by EDS spectrum. The presence of C and Cu in the EDS spectrum arise from Cu grid used for sample specimen. The atomic percentages of Nd in the sample were calculated as (~ 0.1%) which clearly indicates the presence of Nd ion in the TiO_2 nanoparticles.

5. Antibacterial activity

In the present study, the antibacterial activity of pure TiO_2 and Nd doped TiO_2 nanoparticles against staphylococcus aureas (Gram positive) and Escherichia coli (Gram-negative) bacteria were investigated. Antibacterial activity of TiO_2 nanoparticle mainly depends on the presence of reactive oxygen species (ROS). The ROS properties are mainly

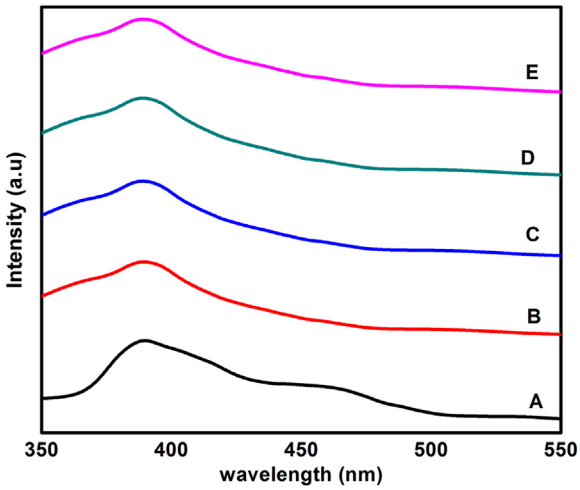

Fig. 4. PL Spectra of (A) Pure TiO_2 (B) 0.5 mM of Nd (C) 1 mM of Nd (D) 1.5 mM of Nd (E) 2 mM of Nd doped TiO_2 Nanoparticles.

due to the smaller in particle size and larger surface area of nanoparticles and increase in oxygen vacancies. The increase in oxygen vacancies results in more reactive oxygen species. ROS is mainly depends on two factors (a) effectiveness of the reactant for diffusion (b) The increase in oxygen vacancies [42]. The superoxide (O_2^-) radicals and hydroxyl radicals (OH.) related to the ROS properties and it can penetrate into the cell membrane and causes damage to DNA and leads to leakage of minerals, protein and genetic material and cell death [43].

The photoactive TiO_2 and Nd doped TiO_2 nanoparticles were used for investigate the antibacterial activity. The electron – hole pair split the water molecules (H_2O) into hydroxyl radicals (OH.) and hydrogen ion (H^+) molecules from the TiO_2 nanoparticles. Dissolved oxygen molecules were converted into superoxide radical anions (O_2^-) and react with hydrogen ion (H^+) to produce (HO_2^-) radicals. These (HO_2^-) radicals collide with electrons and produce hydrogen peroxide anions ($H_2O_2^-$). The hydrogen peroxide (H_2O_2) reacts with H^+ ion to generate hydrogen peroxide molecule. Hydrogen peroxide can interact with the cell wall of bacteria and leads to death [44]. The generation mechanism of free radicals with the help of TiO_2 and water when illuminated with light were given below [45].

$$Ti0_2 + h\nu \rightarrow TiO_2(e^- + h^+) \quad (13)$$

$$H_2O + TiO_2(h^+) \rightarrow TiO_2 + .OH + H^+ \quad (14)$$

$$O_2 + TiO_2(e^-) \rightarrow TiO_2 + .O^- \quad (15)$$

$$O_2^- + H^+ \rightarrow HO_2 \quad (16)$$

$$HO_2^- + H^+ \rightarrow H_2O_2. \quad (17)$$

Fig. 8 shows the various mechanism of antibacterial activity of nanoparticles. The antibacterial activity of TiO_2 nanoparticles further depends on the presence of Ti^{4+} ions and crystallite size of as prepared nanoparticles. The crystallite size was decreases When Nd doped with TiO_2 nanoparticles, which was confirmed by XRD results. Fig. 9(a, b) shows the observed Zone of inhibition of pure TiO_2 and Nd doped TiO_2 nanoparticles for E.Coli and S.aureas. The observed Zone of Inhibition in diameter was increased when doping concentration of Nd increases. This is due to smaller crystallite size. The antibacterial activity of pure TiO_2 and Nd doped TiO_2 nanoparticles against staphylococcus aureas (Gram positive) and Escherichia coli (Gram negative) are shown in the Table 4. In comparison, the antibacterial activity of gram- positive and gram-negative bacteria, the killing effect is higher in Escherichia coli (Gram- negative) than the staphylococcus aureas (Gram- positive) bacteria. The difference in killing effect might be due to variations in cell structure and chemical composition of bacteria. The cell wall of gram-positive bacteria contains thick peptidoglycan and teichoic acid on the outside of plasma membrane. But in the cell wall of gram negative bacteria contains thin peptidoglycan surrounded by

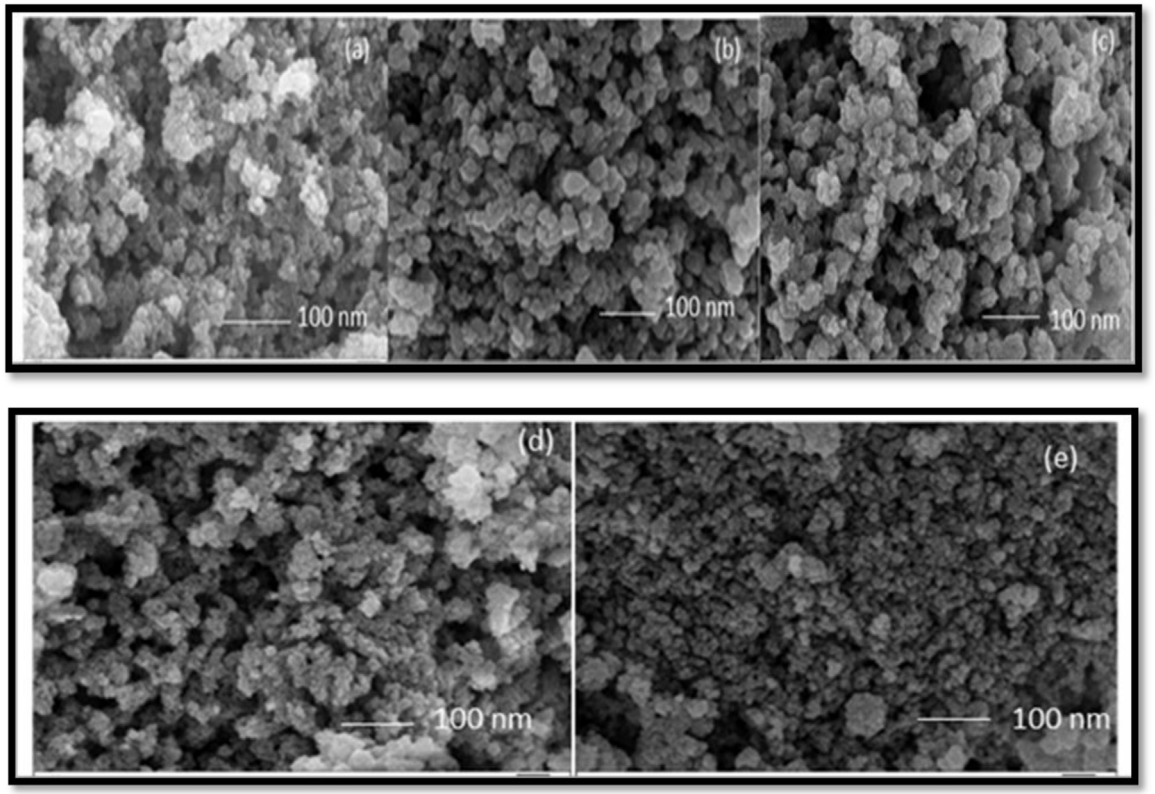

Fig. 5. FESEM images of (a) Pure TiO_2 (b) 0.5 mM of Nd (c) 1 mM of Nd (d) 1.5 mM of Nd (e) 2 mM of Nd doped TiO_2 Nanoparticles.

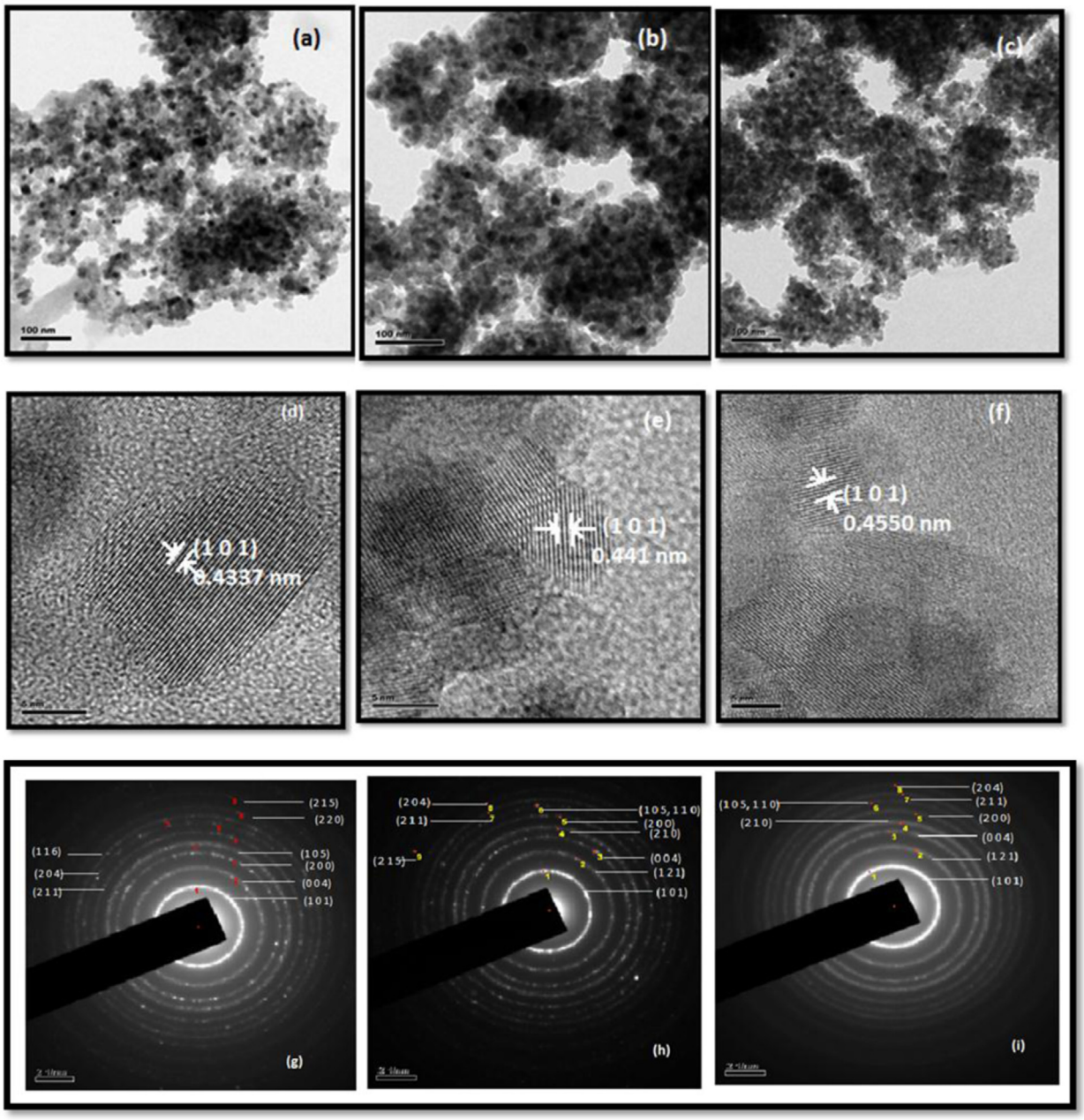

Fig. 6. TEM images of (a) Pure TiO_2 (b) 0.5 mM Nd (c) 2 mM Nd doped TiO_2 Nanoparticles. Lattice fringes of d) Pure TiO_2 e) 0.5 mM of Nd f) 2 mM of Nd doped TiO_2 Nanoparticles. SAED PATTERN of g) Pure TiO_2 h) 0.5 mM of Nd i) 2 mm of Nd doped TiO_2 Nanoparticles.

lipopolysaccharides and it contains negatively charged particles, therefore the titanium ions (Ti^{4+}) were easily capable to attach the sulfhydryl group (SH) of enzymes of bacteria which leads to cell death quickly [46]. Therefore, the killing effect is higher in gram negative bacteria than the gram positive bacteria.

Fig. 10(a, b) shows the antibacterial activity of TiO_2 and Nd doped TiO_2 nanoparticles. From the antibacterial tests, it was concluded that, Nd doped TiO_2 nanoparticles render more effective antibacterial activity than the pure TiO_2 nanoparticles. Moreover, the killing effect of Nd doped TiO_2 nanoparticles increases when the concentration of dopant Nd increases. Because the doping concentration of Nd increases, the crystallite size decreases. The smaller particle size leads to larger surface area. Therefore, it can easily penetrate into the cell wall and leads to cell death. It is also interesting that, the both pure TiO_2 and Nd doped TiO_2 nanoparticles shows good antibacterial activity towards gram-negative bacteria than the gram-positive bacteria. The result clearly indicates that the presence of as prepared nanoparticles leads to the breakages of cell membrane of gram- negative and gram-positive bacteria. The antibacterial activity of TiO_2 nanoparticles (metal oxide compounds) depends on the crystalline nature, particle size, surface area, porosity and oxygen vacancies [47].

6. Photocatalytic activity

When TiO_2 nanoparticles are irradiated by UV light, the electrons in the valence band are excited to conduction band to generate electron – hole pairs [48]. The holes in TiO_2 nanoparticles reacts with water molecules or hydroxide ions and to form hydroxyl radicals. The hydroxyl radicals is a powerful oxidation agent that attack organic pollutants. This process results in the photo oxidation of organic pollutants with the following process:- (i) light adsorption of the photo catalyst (ii) production of electron and hole pairs (iii) recombination of charge

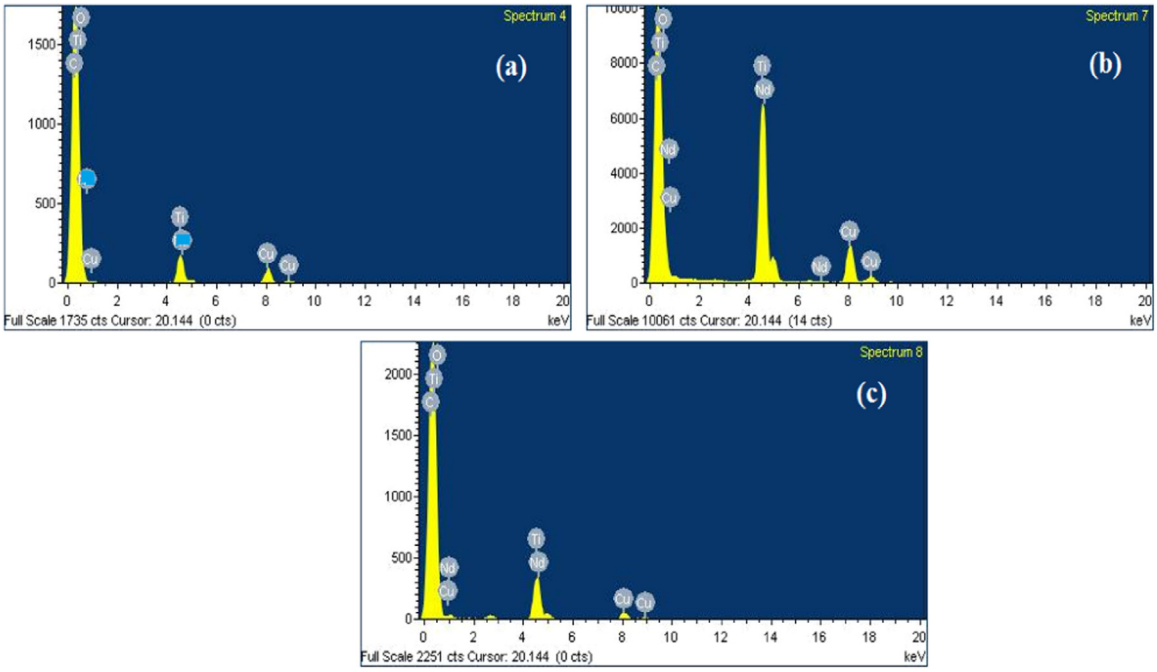

Fig. 7. EDS Spectra of a) Pure TiO_2 b) 0.5 mM of Nd c) 2 mm of Nd doped TiO_2 Nanoparticles.

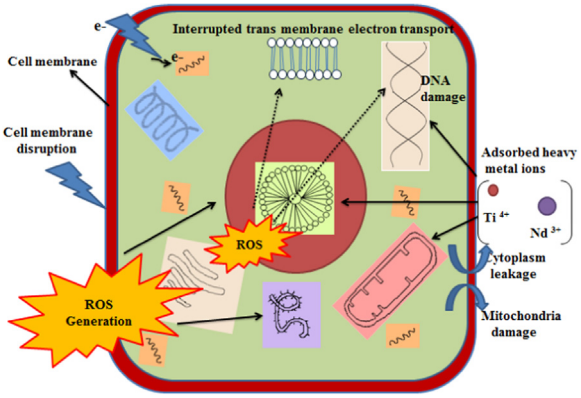

Fig. 8. Typical diagram of mechanism of antibacterial activity of metal ion NPs.

carriers and (iv) usage of charge carriers by the reactants [49]. In addition, large amounts of oxygen vacancies were created when Nd doped with TiO_2 nanoparticles. On the other hand, Nd doped TiO_2 nanoparticles, Nd^{3+} ions can be served as electron scavengers, which may react with super oxide and prevent the electron hole pair recombination process. The mechanism for the improved photocatalytic activity of

Table 4
Inhibition zone diameters of Escherichia coli and Staphylococcus aureas for Pure TiO_2 and Nd doped TiO_2 Nanoparticles.

S.No	Nd concentration	Inhibition zone diameter (mm)	
		E.Coli	S.aureus
1	Control	18	7
2	0.0 mM	20	8
3	0.5 mM	22	9
4	1.0 mM	24	10
5	1.5 mM	26	12
6	2.0 mM	28	13

pure TiO_2 and Nd doped TiO_2 nanoparticles were as follows [50].

$$TiO_2 + \quad h\nu \rightarrow h^+ + e^- \tag{18}$$

$$e^- + O_2 \rightarrow O_2^- \tag{19}$$

$$h^+ + OH^- \rightarrow OH \tag{20}$$

$$O_2^- + 2H^+ \rightarrow 2OH \tag{21}$$

$$OH \quad + \quad \text{dye} \rightarrow \text{Degradation products} \tag{22}$$

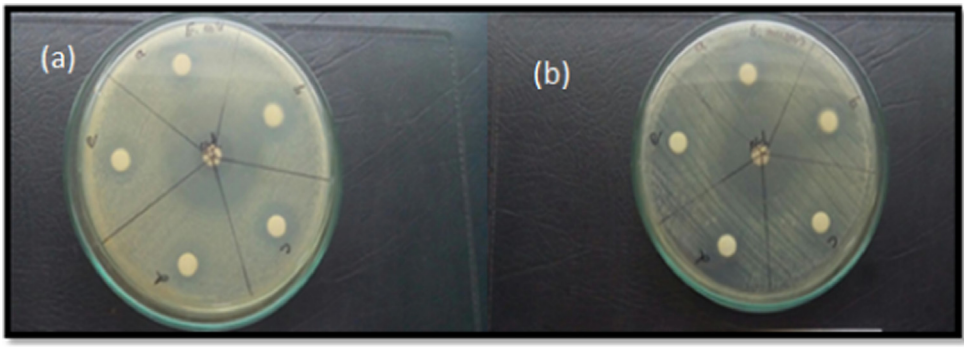

Fig. 9. (a, b) Escherichia coli and Staphylococcus aureas bacteria medium Inhibition zone of a) Pure TiO_2 b) 0.5 mM of Nd c)1 mM of Nd d) 1.5 mM of Nd e) 2 mM of Nd doped TiO_2 Nanoparticles.

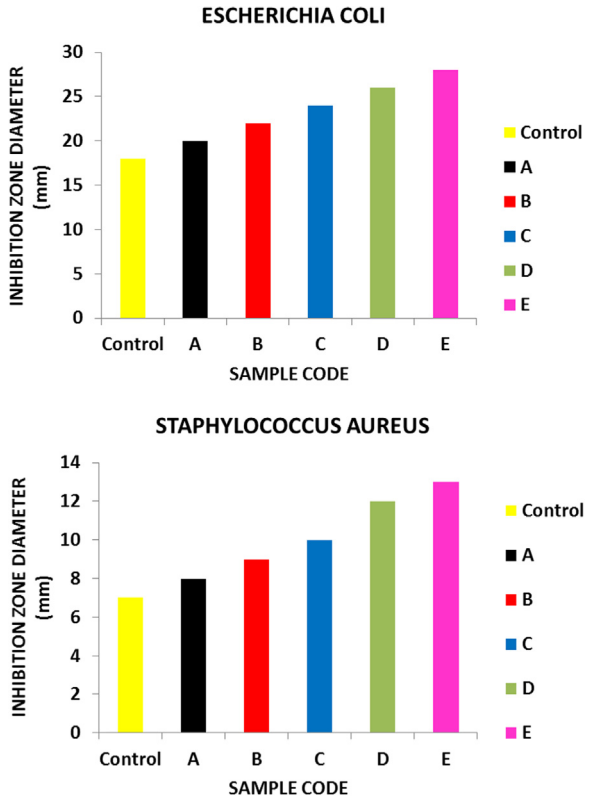

Fig. 10. (a) Size of Zone of inhibition, Control A) Pure TiO_2 B) 0.5 mM of Nd C) 1 mM of Nd D) 1.5 mM of Nd E) 2 mm of Nd doped TiO_2 Nanoparticles. (b) Size of Zone of inhibitions, Control A) Pure TiO_2 B) 0.5 mM of Nd C) 1 mM of Nd D) 1.5 mM of Nd E) 2 mM of Nd doped TiO_2 Nanoparticles.

$$Nd^{3+} + OH^{-} \rightarrow Nd^{2+} + OH \quad (23)$$

$$OH + \text{dye} \rightarrow \text{degraded products} \quad (24)$$

However, photocatalytic activity also depends on crystalline nature of nanoparticles, particle distribution, and surface morphology [51].

Methylene blue (MB) and Congo red (CR) dyes where used as a pollutant for photo degradation. The photocatalytic activities of as prepared samples were carried out by the degradation of dyes in aqueous solution. The degradation of both the dyes was evaluated for pure TiO_2 and Nd doped TiO_2 nanoparticles. The UV- visible spectra of pure TiO_2 and Nd doped TiO_2 (0.5 mM and 2.0 mM of Nd) nanoparticles for Methylene blue (MB) as a function of time were shown in Fig. 11(a- c). It shows that there is no degradation of dye takes place in the absence of irradiation. When irradiation time was increased from 0 to 45 min, the intensity of absorption peaks gradually decreases. This leads to dyes were photo degraded and that the photo degradation was increased when Nd doped with TiO_2 nanoparticle. Fig. 12 shows the photo catalytic efficiency of pure TiO_2 and Nd doped TiO_2 nanoparticles. The photo catalytic efficiency was estimated by the following relation [52].

$$X(\%) = \frac{C_0 - C}{C_0} x100 \quad (25)$$

where X is the photo degradation efficiency, Co is the initial concentration of dye and C is the concentration of time in the suspension after time t. The efficiency of pure TiO_2 and Nd doped TiO_2 nanoparticles (0.5 mM and 2.0 mM of Nd) after 45 min were 74%, 90% and 92%. The efficiency percentage is higher for Nd doped TiO_2 nanoparticles when compared with pure TiO_2 nanoparticles. Fig. 13(a-c) shows the absorption spectra of pure TiO_2 and Nd doped TiO_2 and Nd doped TiO_2 (0.5 mM and 2.0 mM of Nd) nanoparticles for Congo Red dye. The result shows that there is no degradation of dye takes place in the absence of irradiation. When irradiation time was increased from 0 to 30 min, the intensity of absorption peaks gradually decreases. This indicates that the dyes were photo degraded by the as prepared samples and that the photo degradation was increased when Nd doped with TiO_2 nanoparticle. Fig. 14 shows the photo catalytic efficiency of pure TiO_2 and Nd doped TiO_2 (0.5 mM and 2.0 mM of Nd) nanoparticles. The efficiency of pure TiO_2 and Nd doped TiO_2 nanoparticles (0.5 mM and 2.0 mM of Nd) after 30 min were 64%, 72%, 86%. The efficiency percentage is higher for Nd doped TiO_2 nanoparticles when compared with pure TiO_2 nanoparticles. Photocatalytic efficiency is higher for Nd doped TiO_2 nanoparticles (2 mM). Therefore reusability, stability and TOC analysis were done for higher concentration of Nd doped TiO_2 nanoparticles.

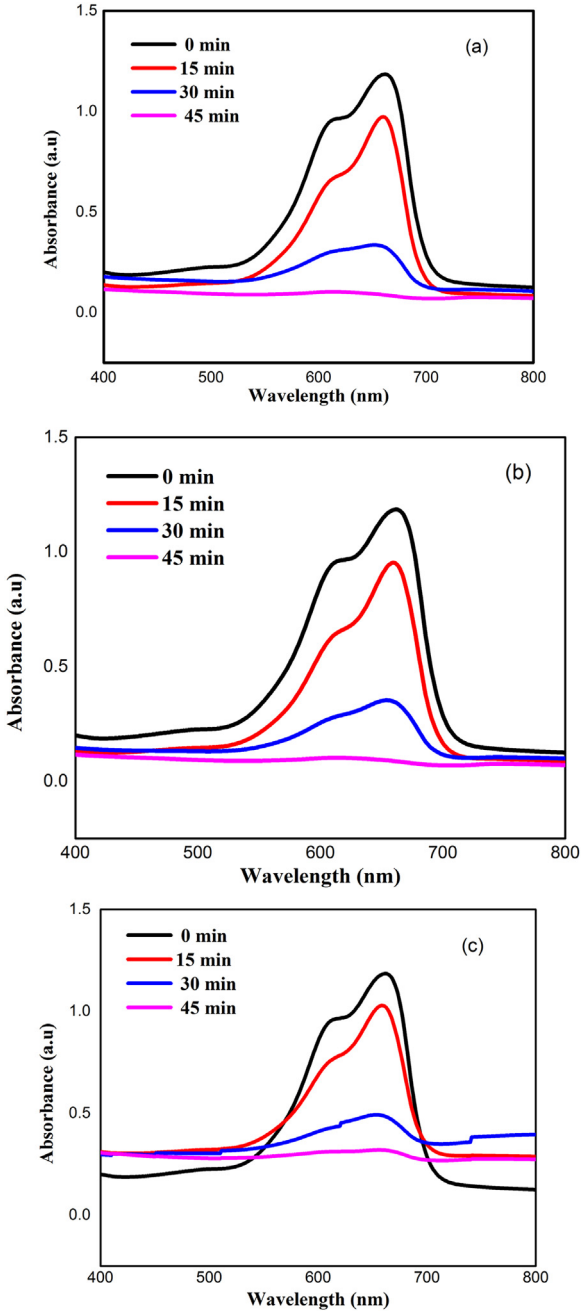

Fig. 11. The UV- visible spectra of (a) Pure TiO_2 (b) 0.5 mM of Nd (c) 2 mM of Nd doped TiO_2 Nanoparticles for Methylene blue (MB) as a function of time.

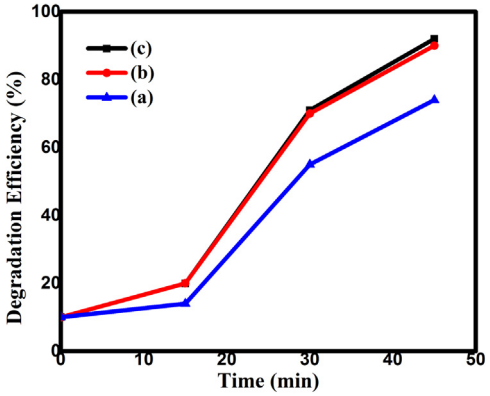

Fig. 12. Degradation Efficiency of (a) Pure TiO_2 (b) 0.5 mM of Nd (c) 2 mM of Nd doped TiO_2 Nanoparticles for Methylene Blue (MR).

6.1. Reusable capacity of the catalyst

For the assessment of re-usability of Nd doped TiO_2 nanoparticles (2 mM) for both MB and CR, it was subjected to consecutive photodegradation of Dye solution under same reaction conditions (20 mg of catalyst +100 ml of dye solution (40 mg/L)). Photocatalyst was recovered after each experiment by centrifugation. The centrifuged photocatalyst was dried in hot-air oven and powdered using Mortar. The photocatalyst was found to be effective even after 5 consecutive photodegradation processes, suggesting that the photocatalyst possess high photocatalytic activity, recoverable and easily reusable. Hence, Nd doped TiO_2 nanoparticles (2 mM) were found to be a better photocatalyst for both dye degradation under UV light illumination.

6.2. Stability of the catalyst

Stability was one of the important factor of photocatalyst. For the effective reuse and regeneration of photocatalyst, it was subjected to photocatalytic reaction using both the dye solution under optimized condition consequentially. The photocatalytic efficiency after utilizing five times was more than 92% for both dyes, which did not significantly decrease and cycle efficiency was shown in Fig. 15. Therefore, the photocatalytic performance of Nd doped TiO_2 nanoparticles (2 mM) was stable and potential for practical application in future.

6.3. Total organic carbon analysis

Total organic carbon (TOC) analysis was accomplished to determine the degree of mineralization of the dye molecules (MB and CR) during the photodegradation process. The degradation process may results in the formation of colorless toxic dye intermediate products [53,54]. This analysis was done by using TOC analyser (Analytikjena/multiN/C3100) for different interval of time up to 3 h with Nd doped TiO_2 nanoparticles (2 mM) because of its highest degradation efficiency. The results of TOC analysis were shown in Fig. 16. The maximum TOC removal was around 86% for MB and 78% for CR. The results also indicates the probability of converting the dye molecules into other intermediate compounds still it exits in the solution irrespective of the degradation of dye which may leads to complete mineralization. The intermediated compounds of dye degradation solution have been reported in lomora et al., i.e hydroxyl and naphthalene (CR) and demethylation intermediate (MB) [55]. In future, this catalyst further doped with any transition metals, biopolymer, or carbon sources for gas sensor applications.

7. Conclusion

The potential applications of TiO_2 nanoparticles such as photocatalytic, antiseptic, antibacterial, and antifungal properties have attracted significant interest in wide range of applications. TiO_2 and Nd doped TiO_2 nanoparticles were synthesized by sol-gel method with different molar ratio of Nd. The characteristics of TiO_2 and neodymium doped TiO_2 nanoparticles were investigated by X-ray diffraction (XRD), UV-Visible Absorption spectroscopy (UV-Vis), Fourier Transforms Infrared spectroscopy (FTIR), Field Emission Scanning Electron Spectroscopy (FESEM), High Resolution Transmission electron Spectroscopy (HRTEM) and Energy Dispersive Spectra (EDS). XRD analysis showed that TiO_2 and Nd doped TiO_2 nanoparticles contains pure anatase, rutile and small brookite tetragonal phase and it further confirmed by TEM. The average crystallite size was about 14–10 nm.

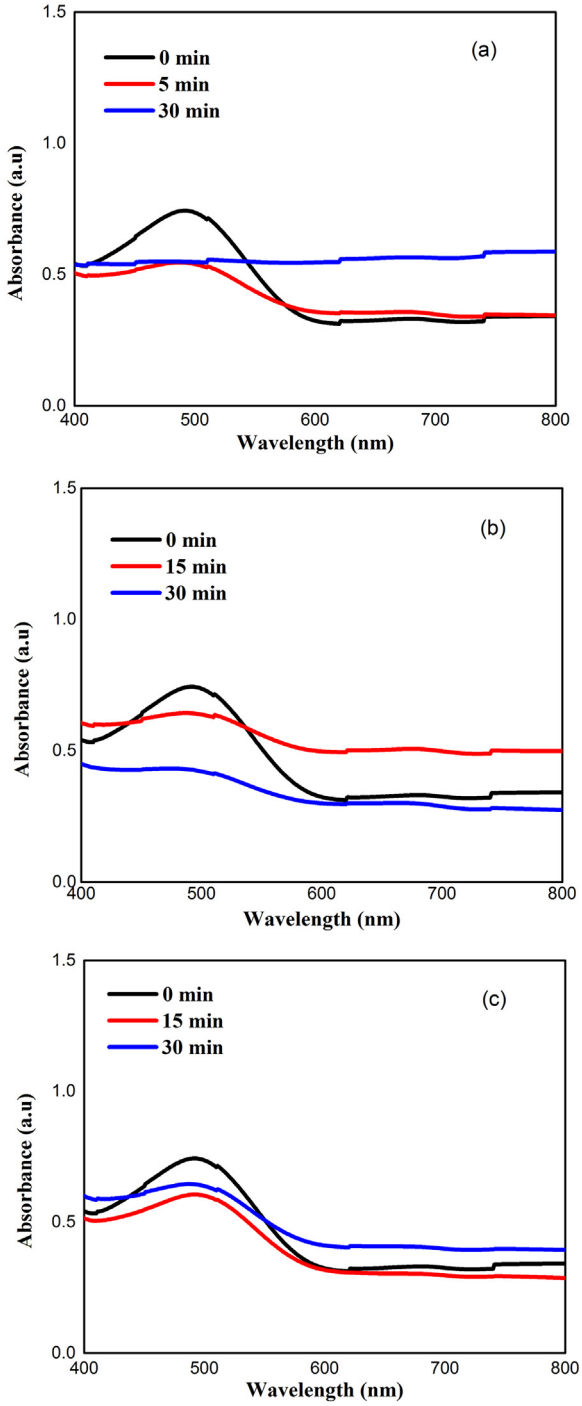

Fig. 13. Absorption spectra of (a) Pure TiO_2 (b) 0.5 mM of Nd (c) 2 mM of Nd doped TiO_2 Nanoparticles for Congo Red (CR).

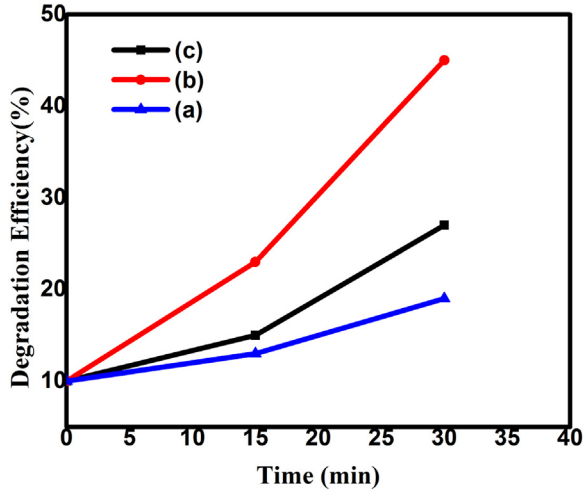

Fig. 14. Degradation efficiency of (a) Pure TiO_2 (b) 0.5 mM of Nd (c) 2 mM of Nd doped TiO_2 Nanoparticles for Congo Red (CR).

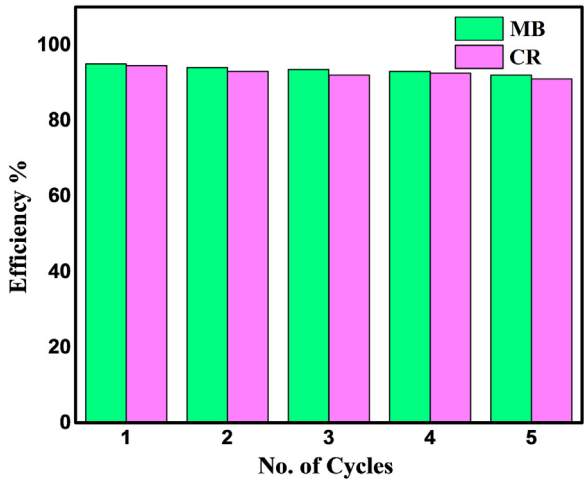

Fig. 15. Stability of Nd doped TiO_2 nanoparticles (2 mM) for MB and CR.

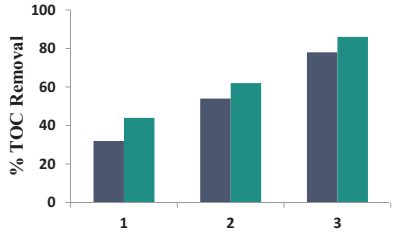

Fig. 16. TOC removal % by Nd doped TiO_2 nanoparticles (2 mM) for MB and CR.

Addition of Nd employed remarkable influence on phase transition of TiO_2 nanoparticles occurred at 600 °C. The optical properties of TiO_2 and Nd doped TiO_2 nanoparticles were confirmed by UV-Visible (UV-Vis) and Photoluminescence (PL) spectroscopy. The increase in absorption peak at UV visible spectra with decrease in PL intensities of Nd doped TiO_2 nanoparticles in comparison with pure TiO_2 nanoparticles. The photocatalytic activity of as prepared TiO_2 and Nd doped TiO_2 nanoparticles were evaluated by photo degradation of methylene blue (MB) and Congo Red (CR) under ultraviolet irradiation. Nd doped TiO_2 enhanced the photocatalytic activity when compared with TiO_2 nanoparticles. The antibacterial activities were studied for Escherichia coli (E.Coli) and Staphylococcus aureas (S.aureas). Nd doped TiO_2 nanoparticles showed good antibacterial activity when compared with TiO_2 nanoparticles. From the photocatalytic and antibacterial activity results, TiO_2 and Nd doped TiO_2 can be used as a photocatalytic active material in wastewater treatment and also used an antibacterial agents.

References

[1] Sunandan Baruah, Samir K. Pal, Joydeep Dutta, Nanostructured zinc oxide for water treatment, Nanosci. Nanotechnol. Asia 2 (2012) 90–102.

[2] Si-Wei Zhao, Chong-Rui Guo, Ying-Zhu Hu, Yuan-Ru Guo, Qing-Jiang Pan, The preparation and antibacterial activity of cellulose/ZnO composite: a review, Open Chem. 16 (2018) 9–20.

[3] Damian Wojcieszak, Michal Mazur, Michalina Kurnatowska, Danuta Kaczmarek, Jaroslaw Domaradzki, Leszek Kepinski, Kamil Chojnacki, Influence of Nd-doping on photocatalytic properties of TiO_2 nanoparticles and thin film coatings, Int. J. Photoenergy (2014) (10 pages).

[4] Saman Jafari, Mohammad Reza Mohammadi, Hamid Reza Madaah Hosseini, Impact of morphology and nitrogen and carbon co-doping on photocatalytic activity of TiO_2 as environmental catalysts, Ind. Eng. Chem. Res. (2016) 12205–12212.

[5] Yi Xie, Sung Hwan Heo, Seung Hwa Yoo, Ghafar Ali, Sung Oh Cho, Synthesis and photocatalytic activity of anatase TiO_2 nanoparticles-coated carbon nanotubes, Nanoscale Res. Lett. 5 (2010) 603–607.

[6] A. Kedziora, W. Strek, L. Kepinski, G. Bugla-Ploskonska, W. Doroszkiewicz, Synthesis and antibacterial activity of novel titanium dioxide doped with silver, J. Sol-Gel Sci. Technol. 62 (2012) 79–86.

[7] Nafise Ebrahim Jasbi, Davoud Dorranian, Effect of aging on the properties of TiO_2 nanoparticle, J. Theor. Appl. Phys. 10 (2016) 157–161.

[8] Alicja Mikolajczyk, Natalia Sizochenko, Ewa Mulkiewicz, Anna Malankowska, Michal Nischk, Przemyslaw Jurczak, Seishiro Hirano, Grzegorz Nowaczyk, Adriana Zaleska-Medynska, Jerzy Leszczynski, Agnieszka Gajewicz, Tomasz Puzyn, Evaluating the toxicity of TiO_2 -based nanoparticles to Chinese hamster ovary cells and Escherichia coli: a complementary experimental and computational approach, Beilstein J. Nanotechnol. 8 (2017) 2171–2180.

[9] Anuja Bokare, Mrinal Pai, A. Anjali, Athawale, Surface modified Nd doped TiO_2 nanoparticles as photocatalysts in UV and solar light irradiation, Sol. Energy 91 (2013) 111–119.

[10] G.V. Khade, N.L. Gavade, M.B. Suwarnkar, M.J. Dhanavade, K.D. Sonawane, K.M. Garadkar, Enhanced photocatalytic activity of europium doped TiO_2 under sunlight for the degradation of methyl orange, J. Mater. Sci. Mater. Electron. 28 (2017) 11002–11011.

[11] M. Shamshi Hassan, Touseef Amna, O.-Bong Yang, Hyun-Chel Kim, Myung-Seob Khil, TiO_2 nanofibers doped with rare earth elements and their photocatalytic activity, Ceram. Int. 38 (2012) 5925–5930.

[12] Jun Du, Xin Gu, Qi Wu, Jiao Liu, Hai-zhi Guo, Jian-guo Zou, Hydrophilic and photocatalytic activities of Nd-doped titanium dioxide thin films, Trans. Nonferrous Met. Soc. 25 (2015) 2601–2607.

[13] Nadia Febiana Djaja, Rosari Saleh, Characteristics and photocatalytics activities of Ce-doped ZnO nanoparticles, Mater. Sci. Appl. 4 (2013) 145–152.

[14] Mohammed A. Hamza, Fawaz N. Saiof, Adnan S. Al-ithawi, Majda A. Ameen, Hanna M. Yaseen, Prepared of Nd: TiO_2 nano particles powder as IR filter via Sol-Gel, Sol-Gel Adv. Mater. Phys. Chem 3 (2013) 174–177.

[15] Michal Mazur, Damian Wojcieszak, Danuta Kaczmarek, Jaroslaw Domaradzki, Grzegorz Zatryb, Jan Misiewicz, Jerzy Morgiel, Effect of the nanocrystalline structure type on the optical properties of TiO_2: Nd (1 at%) Thin films, Opt. Mater. 42 (2015) 423–429.

[16] Rui Tang, Qiwen Jiang, Yanhua Liu, Preparation and study on photocatalytic activity of N-doped TiO_2 decorated N-doped graphene, Procedia Eng. 205 (2017) 573–580.

[17] Jesty Thomas, S. Radhikaa, Minjoong Yoon, Nd3 + -doped TiO_2 nanoparticles incorporated with heteropoly phosphotungstic acid: a novel solar photocatalyst for degradation of 4-chlorophenol in water, J. Mol. Catal. A: Chem. 411 (2016) 146–156.

[18] T.L.R. Hewer, E.C.C. Souza, T.S. Martins, E.N.S. Muccillo, R.S. Freire, Influence of neodymium ions on photocatalytic activity of TiO_2 synthesized by sol – gel and precipitation methods, J. Mol. Catal. A Chem. 336 (2011) 58–63.

[19] G. Vijayaprasath, R. Murugan, S. Palanisamy, N.M. Prabhu, T. Mahalingam, Y. Hayakawa, G. Ravi, Structural, optical and antibacterial activity studies of neodymium doped ZnO nanoparticles, J. Mater. Sci. Mater. Electron 26 (2016) 7564–7576.

[20] Qianqian Wang, Shengli Zhu, Yanqin Liang, Zhenduo Cui, Xianjin Yang, Chunyong Liang, Akihisa Inouea, One step synthesis of size controlled Br-doped TiO_2 nanoparticles with enhanced visible light photocatalytic activity, Mater. Res. Bull. 86 (2016) 248–256.

[21] Douga Nassoko, Yan-Fang Li, Jia-Lin Li, Xi Li, Ying Yu, Neodymium-doped TiO_2 with anatase and brookite two phases: mechanism for photocatalytic activity enhancement under visible light and the role of electron, Int. J. Photoenergy (2012) (10 pages).

[22] Zhiqiao He, Qiaolan Cai, Huiying Fang, Gaohua Situ, Jianping Qiu, Shuang Song, Jianmeng Chen, Photocatalytic activity of TiO_2 containing anatase nanoparticles and rutile nanoflower structure consisting of nanorods, J. Environ. Sci. 25 (2013) 2460–2468.

[23] Renate Rossmanith, Clemens K. Weiss, Jasmin Geserick, Nicola Hu¨sing, Ute Ho¨rmann, Ute Kaiser, Katharina Landfester, Porous anatase nanoparticles with

high specific surface area prepared by miniemulsion technique, Chem. Mater. 20 (2008) 5768–5780.
[24] Dhirendra Kumar Sharma, Kapil Kumar Sharma, Vipin Kumar, Anuradha Sharma, Effect of Ce doping on the structural, optical and magnetic properties of ZnO nanoparticles, J. Mater. Sci. Mater. Electron. 27 (2016) 10330–10335.
[25] Ruby Chauhan, Ashavani Kumar, Ram Pal Chaudhary, Structural and optical characterization of Zn doped TiO_2 nanoparticles prepared by sol – gel method, J. Sol-Gel Sci. Technol. 61 (2012) 585–591.
[26] J. El Ghoul, M. Kraini, L. El Mir, Synthesis of Co-doped ZnO nanoparticles by sol – gel method and its characterization, J. Mater. Sci. Mater. Electron. 26 (2015) 2555–2562.
[27] G. Vijayaprasath, R. Murugan, T. Mahalingam, Y. Hayakawa, G. Ravi, Enhancement of ferromagnetic property in rare earth neodymium doped ZnO nanoparticles, Ceram. Int. 41 (2015) 10607–10615.
[28] Md. Hussain Basha, Neeruganti O. Gopal, Dipak B. Nimbalkar, Shyue-Chu Ke, Phosphorus and boron codoping into TiO_2 nanoparticles; an avenue for enhancing the visible light photocatalytic activity, J. Mater. Sci. Mater. Electron. 28 (2016) 987–993.
[29] B. Rajamannan, S. Mugundan, G. Viruthagiri, N. Shanmugam, R. Gobi, P. Praveen, Preparation, structural and morphological studies of Ni doped titania nanoparticles, Spectrochim. Acta Part A Mol. Biomol. Spectrosc. 128 (2014) 218–224.
[30] Sunil Chauhan, Manoj Kumar, Sandeep Chhoker, S.C. Katyal, V.P.S. Awana, Structural, vibrational, optical and magnetic properties of sol – gel derived Nd doped ZnO nanoparticles, J. Mater. Sci. Mater. Electron. 24 (2013) 5102–5110.
[31] Siddhartha Sankar Boxi, Santanu Paria, Visible light induced enhanced photocatalytic degradation of organic pollutants in aqueous media using Ag doped hollow TiO_2 nanospheres, RSC Adv. (2015) 37657–37668.
[32] Dinkar V. Aware, Shridhar S. Jadhav, Synthesis, characterization and photocatalytic applications of Zn-doped TiO_2 nanoparticles by sol – gel method, Appl. Nanosci. 6 (2016) 965–972.
[33] B. Roya, S. Chakrabartya, O. Mondala, M. Palb, A. Duttaa, Effect of neodymium doping on structure, electrical and optical properties of nanocrystalline ZnO, Mater. Charact. 70 (2011) 1–7.
[34] Nimisha N. Kumaran, K. Muraleedharan, Photocatalytic activity of ZnO and Sr^{2+} doped ZnO nanoparticles, J. Water Process Eng. 17 (2017) 264–270.
[35] Dhanya Chandran, Lakshmi S. Nair, S. Balachandran, K. Rajendra Babu, M. Deepa, Band gap narrowing and photocatalytic studies of Nd^{3+} ion-doped SnO_2 nanoparticles using solar energy, Bull. Mater. Sci. 39 (2016) 27–33.
[36] Laveena P. D'Souza, R. Shwetharani, Vipin Amoli, C.A.N. Fernando, Anil Kumar Sinha, R. Geetha Balakrishna, Photoexcitation of neodymium doped TiO_2 for improved performance in Dye - sensitized solar cells, JMADE 104 (2016) 346–354.
[37] J. El Ghoul, Synthesis of vanadium doped ZnO nanoparticles by sol – gel method and its characterization, J. Mater. Sci. Mater. Electron. 27 (2015) 2159–2165.
[38] Prakash Chand, Anurag Gaur, Ashavani Kumar, Study of optical and ferroelectric behavior of ZnO nanostructures, Adv. Mat. Lett. 4 (2013) 220–224.
[39] Lalitha Gnanasekaran, R. Hemamalini, K. Ravichandran, Synthesis and characterization of TiO_2 quantum dots for photocatalytic application, J. Saudi Chem. Soc. (2015) 1–6.
[40] R.S. Dubey, Shyam Singh, Results in physics investigation of structural and optical properties of pure and chromium doped TiO_2 nanoparticles prepared by solvothermal method, Results Phys. 7 (2017) 1283–1288.
[41] Hemraj Mahipati Yadav, Jung-Sik Kim, Shivaji Hariba Pawar, Developments in photocatalytic antibacterial activity of nano TiO_2: a review, Korean J. Chem. Eng. 32 (2016) 1–10.
[42] S.B. Rana, R.P.P. Singh, Investigation of structural, optical, magnetic properties and antibacterial activity of Ni-doped zinc oxide nanoparticles, J. Mater. Sci. Mater. Electron. 27 (2016) 9346–9355.
[43] Manuela Stan, Adriana Popa, Dana Toloman, Teofil-Danut Silipas, Dan Cristian Vodnar, Antibacterial and antioxidant activities of ZnO nanoparticles synthesized using extracts of allium sativum, Rosmarinus officinalis and Ocimum basilicum, Acta Metall. Sin. Engl. Lett. 29 (2016) 228.
[44] Jitendra Bahadur, Shraddha Agrawal, Vinay Panwar, Azra Parveen, Kaushik Pal, Antibacterial properties of silver doped TiO_2 nanoparticles synthesized via Sol-Gel technique, Macromol. Res. 24 (2016) 488–493.
[45] P.M. Narayanan, Wijo Samuel Wilson, Ashish Thomas Abraham, Murugan Sevanan, Synthesis, characterization, and antimicrobial activity of zinc oxide nanoparticles against human pathogens, BioNanoScience 2 (2012) 329–335.
[46] G.K. Prashanth, P.A. Prashanth, Utpal Bora, Manoj Gadewar, B.M. Nagabhushana, S. Ananda, G.M. Krishnaiah, H.M. Sathyananda, " In vitro antibacterial and cytotoxicity studies of ZnO nanopowders prepared by combustion assisted facile green synthesis, Karbala Int. J. Mod. Sci. 1 (2015) 67–77.
[47] S.K.M. Jose, Streptomycin loaded TiO_2 nanoparticles: preparation, characterization and antibacterial applications, J. Nanostruct. Chem. 7 (2017) 47–53.
[48] Raad S. Sabry, Yousif K. Al-Haidarie, Muhsin A. Kudhier, Synthesis and photocatalytic activity of TiO_2 nanoparticles prepared by sol – gel method, J. Sol-Gel Sci. Technol. 78 (2016) 299–306.
[49] U.G. Akpan, B.H. Hameed, The advancements in sol – gel method of doped-TiO_2 photocatalysts, Appl. Catal. A Gen. 375 (2010) 1–11.
[50] J. Zhang, S.J. Deng, S.Y. Liu, J.M. Chen, B.Q. Han, Y. Wang, Y.D. Wang, Preparation and photocatalytic activity of Nd doped ZnO nanoparticles, Mater. Technol. 7857 (2016) 262–268.
[51] Bing-Lei Guo, Ping Han, Li-Chuan Guo, Yan-Qiang Cao, Ai-Dong Li, Ji-Zhou Kong, Hai-Fa Zhai, Di Wu, The ANtibacterial Activity of Ta-doped ZnO nanoparticles, Nanoscale Res. Lett. 10 (2015) 336.
[52] M. Khairy, W. Zakaria, Effect of metal-doping of TiO_2 nanoparticles on their photocatalytic activities toward removal of organic dyes, Egypt. J. Pet. 23 (2014) 419–426.
[53] Samuel Osei-Bonsu Oppong, William W. Anku, Sudheesh K. Shukla, Eric S. Agorku, Poomani P. Govender, Photocatalytic degradation of indigo carmine using Nd-doped TiO_2-decorated graphene oxide nanocomposites, J. Sol-Gel Sci. Technol. 80 (2016) 38–49.
[54] William Wilson Anku, Samuel Osei-Bonsu Oppong, Sudheesh Kumar Shukla, Poomani Penny Govender, Comparative photocatalytic degradation of monoazo and diazo dyes under simulated visible light using Fe3+/C/S doped-TiO_2 nanoparticles, Acta Chim. Slov. 63 (2016) 380–391.
[55] M. Lomoră, C. Drăghici, Al Eneşca, Intermediary compounds in advanced oxidation processes for wastewater treatment, Bull. Transilv. 4 (2011) 53.